10^{th} International Conference on Fracture Mechanics of Concrete and Concrete Structures
FraMCoS-X
G. Pijaudier-Cabot, P. Grassl and C. La Borderie (Eds)
https://doi.org/10.21012/FC10.235604

SIMULATIONS OF SPLIT HOPKINSON PRESSURE BAR BY DISCRETE MESOSCALE MODEL

JOSEF KVĚTOŇ* AND JAN ELIÁŠ*

*Brno University of Technology
Czech Republic
e-mail: kveton.j@fce.vutbr.cz, jan.elias@vut.cz

Key words: Particle model, Concrete fracture, Strain-rate, Dynamics

Abstract. The contribution presents simulations of concrete fracture under high strain rates. For relatively low rates (below 0.1 m/s) rate dependency is attributed mostly to creep phenomenon, whereas for higher rates the leading phenomenon is inertia. Discrete meso-scale model is used to represent material behavior. Thanks to the explicit representation of mesoscale structure, the main inertia effects should be captured automatically. However, the inertia due to smaller omitted particles must be phenomenologically represented as a rate dependent component of the constitutive relation. In the presented study, several model parameters settings are investigated and the results of the numerical simulations are compared with the experimental evidence.

1 INTRODUCTION

The concrete fracture is phenomenon studied in detail for several decades. Its characteristic quasi-brittle and size dependent behavior brings complications that make investigations challenging. Another difficulty is rate dependency of the behavior. It is well understood that the resistance of material increases with increasing loading rate [1]. This behavior is attributed to several phenomena, major one at high loading rates being the inertia. Usual way to describe the rate effects is via dynamic increase factor (DIF).

Experimental data regarding increase in compressive strength are quite abundantly reported in literature already since the half of 20th century, e.g. [12]. On the other hand, data qualifying tensile strength of concrete under different strain-rates, especially when concerning more information than simply dynamic tensile strength, are quite limited.

Using conventional techniques for testing of concrete tensile properties (e.g. uni-axial tensile test), one is limited by the presence of supports, more precisely by their unsatisfying toughness. For example experiments on concrete L-shape corners or compact tension tests can be found in [15]. These test are performed in dynamic regime under relatively low loading rates, up to 2.4 m/s.

More convenient technique was reported e.g. in [10] where long concrete bar was first loaded in compression along the bar length, and simultaneously biaxial compression was applied in radial direction. After that, compressive force was released immediately by an explosive (decrease from pre-stressing force to zero happened during period of $3 \cdot 10^{-5}$ s) and as the relaxing wave approached from both sides, it meets in the middle where tensile failure occurs.

Another technique called Split Hopkinson Pressure Bar (SHPB) [2] is based on imposing pressure on a concrete bar that finally breaks in tension after the wave is reflected at the rear face into a tensile stress wave. Several techniques for estimation of dynamic tensile strength by SHPB are reported in literature, e.g. using a distance where failure occurs or various techniques based on observation of specimen velocity field. Simulations of SHPB test by similar discrete model with rate dependency due to viscous material model are reported in [11].

Large set of SHPB experiments is published in [8], including velocity of the rear face of the specimen. These experimental data are chosen for comparison with the presented numerical model.

2 MATHEMATICAL MODEL

2.1 Spatial domain discretization

Concrete fracture takes place at the scale, where one can distinguish individual aggregates. Material is far from homogeneous at this scale. It is therefore convenient to use some model that account for material heterogeneity, such as discrete meso-scale model used here.

The domain is divided into convex polyhedral particles that represent larger aggregates with surrounding cement matrix. Smaller aggregates are not considered explicitly, but their effect is smeared into the constitutive model of interparticle interaction. Particle shape is obtained from Voronoi tessellation applied on a set of points randomly placed within a volume domain with a prescribed minimum distance.

2.2 Constitutive relations

Interaction of particles is governed by the constitutive law that is applied at contact facets between neighboring particles. The contact strains at facets are obtained from rigid body kinematics and projected into facet normal (e_N) and tangential (e_M, e_L) directions. Stresses (s_i) in corresponding directions are then calculated with help two elastic material parameters, namely meso-scale elastic modulus E_0 and tangential to normal stiffness ratio α, and damage variable D.

$$s_i = (1-D)E_i e_i \quad \text{for} \quad i = N, M, L \tag{1}$$

$$E_N = E_0,\ E_{M,L} = \alpha E_0 \tag{2}$$

In linearly elastic regime when $D = 0$, macroscopic Young's modulus E and Poisson's ratio ν can be approximately derived through principle of virtual work [6] and then relation between meso and macroscopic parameters reads

$$E_0 = \frac{E}{1-2\nu} \qquad \alpha = \frac{1-4\nu}{1+\nu} \tag{3}$$

Damage parameter is responsible for nonlinear effects. It is evaluated according to paper of G. Cusatis [4] using additional model parameters. We consider two of them (mesoscopic fracture energy G_f and tensile strength f_t) as governing parameters in inelastic regime, the other material constants are derived from these two. The model from [4] is further simplified by neglecting confinement effect. Reader interested in detailed description is referred to [5]. Anisotropic nature of concrete fracture is captured thanks to random geometry of particle system.

2.3 Transient solution

Simulations of material behavior under high strain-rates bring necessity of dynamic solution. Equations of motion are solved using an implicit time integration scheme according to Newmark [13], then using numerical time-derivatives of accelerations and velocities according to Eqs. (5) and (6), system of equations stated in Eq. (4) is obtained

$$\begin{aligned}\left(\boldsymbol{K} + \frac{1}{\beta\Delta t^2}\boldsymbol{M} + \frac{\gamma}{\beta\Delta t}\boldsymbol{C}\right)\boldsymbol{u}_{t+\Delta t} = \;& \boldsymbol{F}_{t+\Delta t} + \boldsymbol{M}\left(\tfrac{1}{\beta\Delta t^2}\boldsymbol{u}_t + \tfrac{1}{\beta\Delta t}\dot{\boldsymbol{u}}_t + \left(\tfrac{1}{2\beta}-1\right)\ddot{\boldsymbol{u}}_t\right) + \\ & + \boldsymbol{C}\left(\tfrac{\gamma}{\beta\Delta t}\boldsymbol{u}_t + \left(\tfrac{\gamma}{\beta}-1\right)\dot{\boldsymbol{u}}_t + \tfrac{\Delta t}{2}\left(\tfrac{\gamma}{\beta}-2\right)\ddot{\boldsymbol{u}}_t\right)\end{aligned} \tag{4}$$

$$\ddot{\boldsymbol{u}}_{t+\Delta t} = \tfrac{1}{\beta\Delta t^2}\left(\boldsymbol{u}_{t+\Delta t} - \boldsymbol{u}_t\right) - \tfrac{1}{\beta\Delta t}\dot{\boldsymbol{u}}_t - \left(\tfrac{1}{2\beta}-1\right)\ddot{\boldsymbol{u}}_t \tag{5}$$

$$\dot{\boldsymbol{u}}_{t+\Delta t} = \dot{\boldsymbol{u}}_t + \Delta t\left(1-\gamma\right)\ddot{\boldsymbol{u}}_t + \gamma\Delta t\ddot{\boldsymbol{u}}_{t+\Delta t} \tag{6}$$

where $\boldsymbol{M}$, $\boldsymbol{C}$ and $\boldsymbol{K}$ are mass, damping and stiffness matrices respectively, $\boldsymbol{F}$ and $\boldsymbol{u}$ are loading and displacement vector. Dotted symbol denotes time derivative. β and γ are parameters of the Newmark method. In the presented model, the system is damped only in nonlinear regime by dissipation of energy due to fracture. Additional damping by matrix $\boldsymbol{C}$ is omitted.

2.4 Rate dependency

The model represents explicitly only the largest mineral aggregates. It is therefore necessary to capture the material behavior under this scale phenomenologically in constitutive relation. To account for inertia of the interparticle material, the constitutive behavior of contact facets is enriched by dependency on difference in velocities of particles it connects. Following strain rate dependent function from [3] is adopted and mechanical behavior of every contact is then scaled accordingly.

$$F(\dot{e}) = 1 + c_1 \text{arcsinh}\left(\frac{\dot{e}l}{c_0}\right) \tag{7}$$

where e is mesoscopic equivalent strain, l is distance between contacting particle centers and c_0 and c_1 are additional material properties. Initial slope of the softening curve remains unchanged, therefore more energy is dissipated. This accounts for less localized strain in material volume that is under resolution of the model compared to quasi-static fracture.

3 DYNAMIC TENSILE STRENGTH

3.1 Split Hopkinson pressure bar

The test setup consists of long metal (usually steel or aluminum alloy) bar and relatively short concrete cylinder at its end. Metal bar is loaded by impact of a projectile or by an explosive and the pressure wave propagates along the bar until it reaches its end. At the contact between metal and concrete, some part of pressure wave is reflected backwards to the metal bar as a tensile wave and the rest of it is transmitted into the concrete specimen, where it further propagates as a pressure wave. When it reaches the rear face of concrete cylinder, it is reflected as a tensile wave and, after reaching the material tensile strength, the specimen breaks.

To determine the dynamic tensile strength from results of SHPB test, theory derived for 1D longitudinal wave propagation according to [14] is usually applied. In [7], the following relation is stated.

$$f_{\text{t,dyn}} = \frac{1}{2}\,\rho\, c\, \Delta V_{\text{pb}} \tag{8}$$

where E and ρ are macroscopic elastic modulus and density respectively and ΔV_{pb} is pullback velocity, which is difference between the maximum and “residual” velocity of the rear face of the specimen. c is wave velocity, which can be, in case of elastic material analytically achieved from the following relation

$$c = \sqrt{\frac{E(1+\nu)}{\rho(1+\nu)(1-2\nu)}} \tag{9}$$

3.2 Experimental data for comparison

To validate the model, series of experimental data has been searched in literature. Test series reported in [7,8] was selected because of its complexity and direct measurements of the rear face velocity, which is important for estimation of dynamic tensile strength.

It was a large series of specimens tested using not only SHPB setup, but also tensile test performed in conventional apparatus to determine material properties under lower and quasi-static strain-rates.

Two tests were selected for comparison with results of the developed numerical model. Stress waves transmitted from aluminum alloy bar of length $1.2\,\text{m}$ reported in [8] are plotted in Fig. 1. The maximum strain-rate calculated from the stress waves is $41/\text{s}$ and $94/\text{s}$ for wave 1 and 2 respectively.

Concrete specimen had length $L = 140\,\text{mm}$ and radius $R = 22.5\,\text{mm}$. Specimens were made of saturated (wet) concrete with the following macroscopic parameters: elastic modulus $E = 42\,\text{GPa}$, Poisson's ratio $\nu = 0.2$, density $\rho = 2380\,\text{kg/m}^3$ and tensile strength $f_\text{t} = 3.7\,\text{MPa}$.

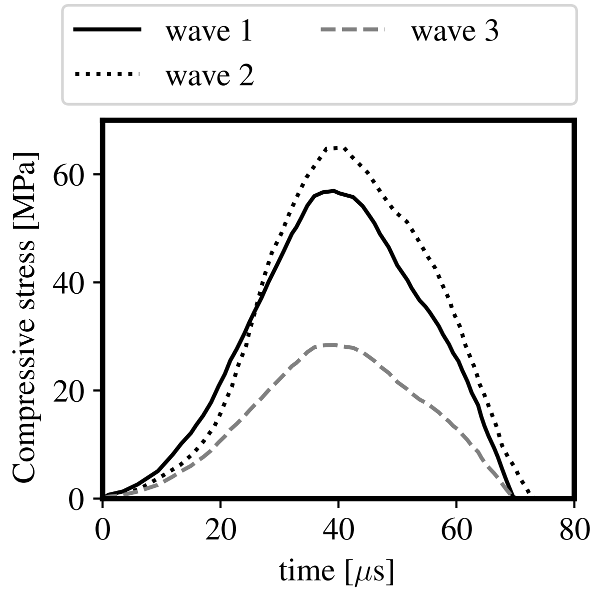

Figure 1: Two stress waves reported in [8], the third wave of half intensity of wave 1 is introduced for preliminary study of model behavior.

4 NUMERICAL SIMULATIONS

4.1 Model setup

The geometry of the model is set according to experimental data from [8]. Concrete specimen is modeled, alloy bar is represented by a stress pressure wave as depicted in Fig. 2. Stress waves used in simulations in following sections are plotted in Fig. 1. wave 1 and 2 correspond to experimental data and wave 3 with half intensity of wave 1 is used for preliminary study.

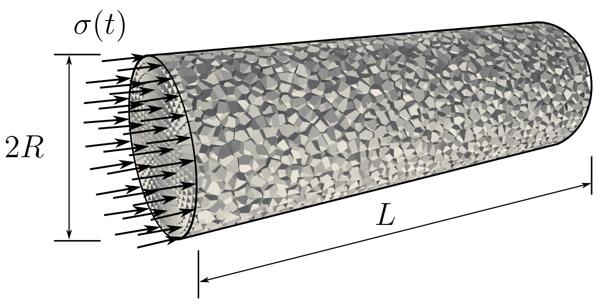

Figure 2: Visualization of model geometry used in numerical simulation of HSB test – concrete cylinder discretized into particles loaded by a stress wave.

4.2 Preliminary study

Focus of this subsection is on behavior of the numerical model. For this purpose, influence of its input parameters on results is investigated. Compressive stress wave imposed on the front face of the specimen is chosen smaller (see Fig. 1) than in case of those reported in experimental series by Erzar & Forquin in [8] in order to reduce inelastic behavior under compression. Note that even for this reduced pressure wave, the strain-rate reaches value $20/\mathrm{s}$.

Material parameters for this preliminary study are following: $E_0 = 70\,\mathrm{GPa}$, $\alpha = 0.237$, $\rho = 2340\,\mathrm{kg/m^3}$, $f_\mathrm{t} = 8\,\mathrm{MPa}$ and $G_\mathrm{f} = 36.5\,\mathrm{N/m^2}$ (for interpretation, see sec. 2.2). Parameters of rate dependency of constitutive law are chosen according to recommendations in [3] $c_0 = 10^{-5}\,\mathrm{s}^{-1}$ and $c_1 = 5 \cdot 10^{-2}$.

The reason for increasing the material strength and use of lower pressure intensity is to avoid material damage in stage of compressive wave. Even though the strength increases due to strain-rate dependency, tensile damage occurs in transverse direction. This damage causes energy dissipation leading to reduction of wave intensity and also changes material behavior. Therefore it strongly affects obtained results.

The rear face velocity in time is plotted in Fig. 3 for 6 different material models. At first, elastic model response was calculated. From this simulation, the value of actual wave speed was obtained as $c_\mathrm{act} = 4340\,\mathrm{m/s}$. Then, the inelastic reference simulation was computed with material parameters mentioned above. Finally, four more material models were considered with (i) fracture energy decreased to one half, (ii) & (iii) tensile strength decreased to one half and one quarter and (iv) eliminated strain rate dependency. For rate independent constitutive law and simulation with lower tensile strength applied, significant amount of damage occurs during propagation of pressure wave which leads to deviation of response from the elastic one already before peak velocity is reached.

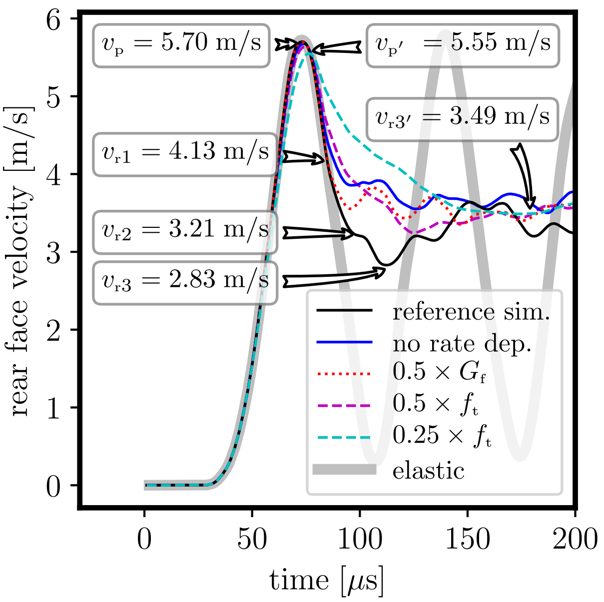

Figure 3: Preliminary study of model behavior – influence of individual material properties.

The dynamic tensile strength is estimated using Eq. (8). Looking at the rear face velocity for reference simulation, it is unclear what value should be taken as so-called "pull-back" velocity ΔV_{pb}. For this purpose, difference between peak (v_p) and residual (v_r) velocity is calculated in three variants as shown in Fig.3. The resulting dynamic strengths can be found in Tab. 1.

i	v [m/s]	ΔV_{pb} [m/s]	$f_{t,dyn}$ [MPa]
v_p	5.70		
v_{r1}	4.13	1.57	7.97
v_{r2}	3.21	2.49	12.64
v_{r3}	2.83	2.87	14.57
$v_{p'}$	5.55		
$v_{r3'}$	3.49	2.06	10.31

Table 1: Different $f_{t,dyn}$ according to three variants of residual velocity v_r

In the first variant, v_{r1} is taken at the point where nonlinear model response start to deviate from the elastic one. The value of dynamic tensile strength in this case $f_{t,dyn} = 7.97$ MPa is close to quasi-static strength. In the remaining variants, v_{r2} and v_{r3} are measured at the first significant kink and at the first local minimum of pullback velocity corresponding to dynamic strength 12.64 and 14.57 MPa. Comparing these values with stress profile at the time when maximum tensile stress was reached (Fig. 4), the v_{r2} variant is more appropriate.

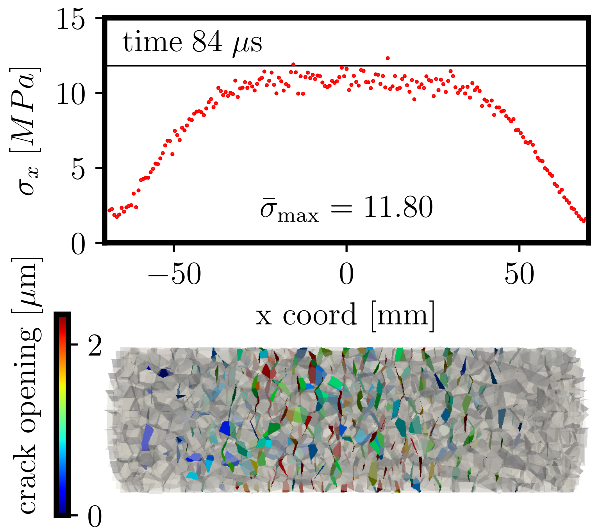

Figure 4: Stress profile along the specimen and crack pattern in time of maximum tensile σ_x for reference simulation.

Focusing on response of the model with reduced fracture energy G_f, there is only one point to consider. Note that the beginning of deviation from elastic response coincides with reference nonlinear simulation, thus this point should be dependent only on value of material strength used (applying the same rate-dependency parameters). However, the residual velocity is different and so is the dynamic tensile strength according to Eq. (8).

Now let us focus on the responses of model using lower value of material tensile strength $0.5 \times f_t$ and $0.25 \times f_t$. From the graph in Fig. 3, one can observe that these curves are deviating from the elastic one already before the peak velocity is reached. The trend is emphasized in case of 25% reference tensile strength. What value should be taken into consideration as residual velocity? The point of deviation from the elastic curve does not even make sense in this case and there is no significant change in the slope of the curve as in case of the reference simulation, so the value $v_{r3'}$ in the lowest point is considered. The resulting dynamic strength is calculated in Tab. 1. Such value is however largely exaggerated, because the real maximum stresses in the specimen are only about 4 Mpa, see Fig 5. We can observe from crack pattern at the same figure that at the time of reaching the maximum tensile stress there is large portion of volume already damaged. This damage happened during the pressure wave propagation and it caused the deviation from the elastic response already before the peak velocity was reached. This corresponds with the recommendation reported in [9] which states that one should avoid pressures larger than 30% of compressive strength.

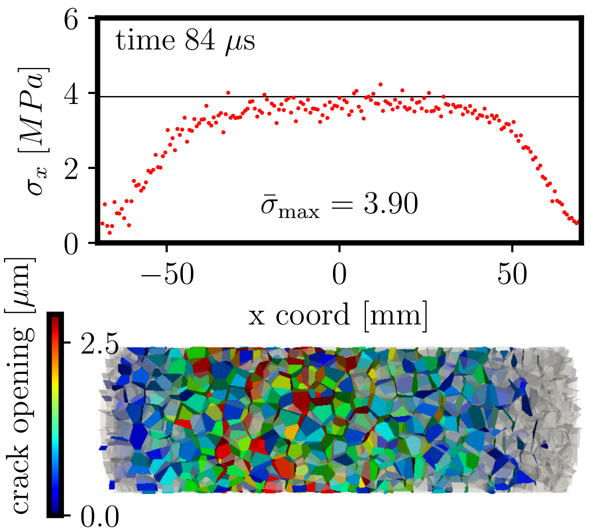

Figure 5: Stress profile along the specimen and crack pattern in time of maximum tensile σ_x for simulation with $0.25 \times f_t$

4.3 Comparison to experimental data

The experiments loaded by pressure wave 1 and 2 are simulated and results compared to the experimental data reported in [8]. Since the relation between macro and mesoscopic elastic properties – Eq. (3) – is only approximate, the actual mesoscale elastic modulus was identified from the wave speed and the maximum velocity of the rear face using *wave 1*. The resulting value $E_0 = 77$ GPa is slightly higher than 70 GPa which would be value obtained by Eq. (3). This is in agreement [5], because Eq. (3) underestimates E_0 for positive Poisson's ratios. For verification, results of elastic FEM simulation with the measured material macroscopic elastic modulus and Poisson's ratio (see sec. 3.2) is performed. The difference between continuous and discrete elastic simulation is negligible for both waves (Fig. 6) and the difference is attributed to different solution methods. The continuous model used explicit time integration, while discrete model integrated in implicit scheme which suffers by numerical damping. The remaining material parameters responsible for inelastic and rate dependent behavior are listed in Tab. 2. The model response for both loading cases along with experimental data from [8] is shown in Fig. 6.

Table 2: Parameter values of numerical model.

elastic modulus	E_0	77 GPa
tang./normal ratio	α	0.1667
density	ρ	2380 kg/m^3
tensile strength	f_t	3.7 MPa
fracture energy	G_f	36.5 N/m^2
rate parameters	c_0, c_1	10^{-5} s^{-1}, 10^{-1}

It can be observed that the experimental peak velocity for wave 1 corresponds to the elastic response of the model. However, looking at the response for wave 2, the model elastic response of the same material is above the experimental peak velocity. It could possibly be explained by inelastic effects occurring in experiments during the pressure wave propagation, which did not occur under lower pressure of wave 1.

The responses of nonlinear model deviates from elastic response in both cases, again due to inelastic effects during compression phase. These effects are magnified when rate dependency is neglected. The descending part of the simulated pullback velocity line is not as steep as reported in experiments. There are multiple macrocracks created in the model, shown in the bottom part Fig. 6, which corresponds to the experimental evidence from [8].

5 CONCLUSIONS

The presented contribution showed numerical simulations of the SHPB tests. Initially, a study of effects of the main model parameters

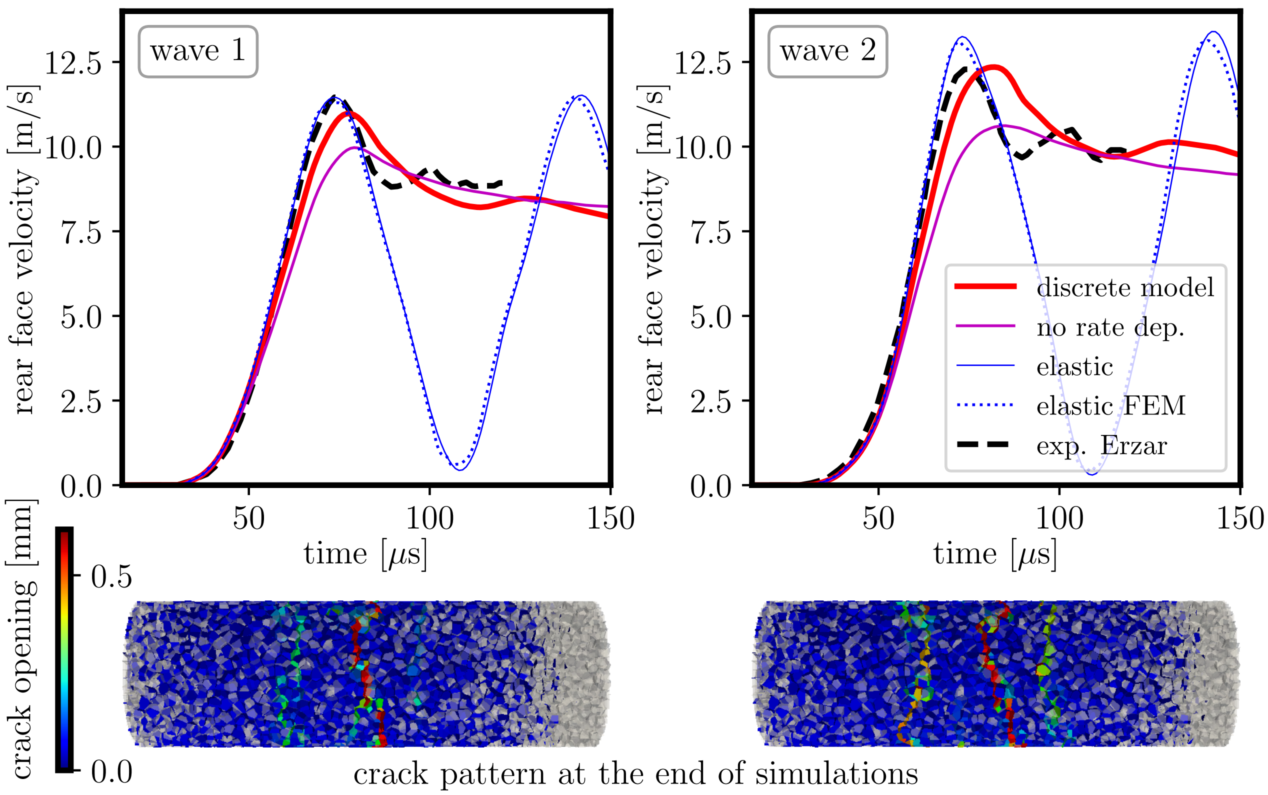

Figure 6: Results of numerical simulations compared to the experimental data from [8].

was investigated. The large effect of inelastic material behavior during pressure wave propagation was described. It was also discussed what value of residual pullback velocity should be used. The most convenient is according to this study velocity at the first kink, the first local minimum might provide exaggerated dynamic strength. Difficulty in determining the residual velocity is caused by inelastic material behavior during the pressure phase as well. We therefore support recommendation from [9] to avoid pressures larger than 30% of compressive strength in the SHPB tests.

The comparison of the model response to the experimental data showed differences due to excessive fracturing during the compression phase. The strain rate dependency of the model constitutive relation helps to reduce these inelastic effect, but only partially.

Acknowledgement

Financial support provided by the Czech Science Foundation under project No. GA19-12197S is gratefully acknowledged.

REFERENCES

[1] *CEB-FIP MODEL CODE*, chapter 2. Material Properties, pages 33–81. 1990.

[2] A. Brara and J.R. Klepaczko. Experimental characterization of concrete in dynamic tension. *Mechanics of Materials*, 38(3):253–267, 2006.

[3] G. Cusatis. Strain-rate effects on concrete behavior. *International Journal of Impact Engineering*, 38(4):162–170, 2011.

[4] G. Cusatis and L. Cedolin. Two-scale study of concrete fracturing behavior. *Engineering Fracture Mechanics*, 74(1-2):3–17, 2007.

[5] Jan Eliáš. Boundary layer effect on behavior of discrete models. *Materials*, 10(2):157, 2017.

[6] J. Eliáš. Adaptive technique for discrete models of fracture. *International Journal of Solids and Structures*, 100–101:376–387, 2016.

[7] B. Erzar and P. Forquin. An experimental method to determine the tensile strength of concrete at high rates of strain. *Experimental Mechanics*, 50(7):941–955, 2010.

[8] B. Erzar and P. Forquin. Experiments and mesoscopic modelling of dynamic testing of concrete. *Mechanics of Materials*, 43(9):505–527, 2011.

[9] P. Forquin, W. Riedel, and J. Weerheijm. Chapter 6 - dynamic test devices for analyzing the tensile properties of concrete. In Jaap Weerheijm, editor, *Understanding the Tensile Properties of Concrete*, Woodhead Publishing Series in Civil and Structural Engineering, pages 137 – 181. Woodhead Publishing, 2013.

[10] J. K. Gran, L. Seaman, and Y. M. Gupta. Application of a new technique to study the dynamic tensile failure of concrete. *Le Journal de Physique Colloques*, 46(C5):C5–617–C5–622, 1985.

[11] Young Kwang Hwang, John E. Bolander, and Yun Mook Lim. Simulation of concrete tensile failure under high loading rates using three-dimensional irregular lattice models. *Mechanics of Materials*, 101:136–146, 2016.

[12] F.M. Mellinger and D.L. Birkimer. Measurements of stress and strain on cylindrical test specimens of rock and concrete under impact loading. Technical report, Ohio River Div Labs Cincinnati, 1966.

[13] N. Newmark. *A method of computation for structural dynamics*. University of Illinois, Urbana, 1959.

[14] S.A. Novikov, I.I. Divnov, and A.G. Ivanov. Investigation of the fracture of steel, aluminum and copper during explosive loading. *Fiz Metallov Metalloved*, 21(4):608–615, 1966.

[15] J. Ožbolt, A. Sharma, and N. Bede. Dynamic fracture of L and CT concrete specimens. *Proceedings of the 9th International Conference on Fracture Mechanics of Concrete and Concrete Structures*, 2016-5-29.